ISSN 1674-1056
http://cpb.iphy.ac.cn
http://iopscience.iop.org/cpb
中国物理 B
Chinese Physics
中国物理 Chinese Physics B

Effect of pressure on the elastic properties and optoelectronic behavior of $Zn_4B_6O_{13}$:First-principles investigation

Pei-Da Wang(王培达), Zhen-Yuan Jia(贾镇源), Yu-Han Zhong(钟玉菡), Hua-Yue Mei(梅华悦), Chun-Mei Li(李春梅), Nan-Pu Cheng(程南璞)
Citation: Chin. Phys. B . 2018, 27(5): 057101. **doi:** 10.1088/1674-1056/27/5/057101

Journal homepage: http://cpb.iphy.ac.cn; http://iopscience.iop.org/cpb

What follows is a list of articles you may be interested in

Magnetism, optical, and thermoelectric response of $CdFe_2O_4$ by using DFT scheme

Q Mahmood, M Yaseen, K C Bhamu, Asif Mahmood, Y Javed, Shahid M Ramay
Chin. Phys. B . 2018, 27(3): 037103. **doi:** 10.1088/1674-1056/27/3/037103

Structural, electronic, and mechanical properties of cubic TiO_2: A first-principles study

Debashish Dash, Chandan K Pandey, Saurabh Chaudhury, Susanta K Tripathy
Chin. Phys. B . 2018, 27(1): 017102. **doi:** 10.1088/1674-1056/27/1/017102

Tuning electronic properties of the S_2/graphene heterojunction by strains from density functional theory

Jun-Hui Lei(雷军辉), Xiu-Fen Wang(王秀峰), Jian-Guo Lin(林建国)
Chin. Phys. B . 2017, 26(12): 127101. **doi:** 10.1088/1674-1056/26/12/127101

Strain engineering of electronic and magnetic properties of Ga_2S_2 nanoribbons

Bao-Ji Wang(王宝基), Xiao-Hua Li(李晓华), Li-Wei Zhang(张利伟), Guo-Dong Wang(王国东), San-Huang Ke(柯三黄)
Chin. Phys. B . 2017, 26(5): 057102. **doi:** 10.1088/1674-1056/26/5/057102

Stability, electronic structures, and mechanical properties of Fe-Mn-Al system from first-principles calculations

Ya-Hui Liu(刘亚会), Xiao-Yu Chong(种晓宇), Ye-Hua Jiang(蒋业华), Jing Feng(冯晶)
Chin. Phys. B . 2017, 26(3): 037102. **doi:** 10.1088/1674-1056/26/3/037102

Effect of pressure on the elastic properties and optoelectronic behavior of $Zn_4B_6O_{13}$: First-principles investigation*

Pei-Da Wang(王培达), Zhen-Yuan Jia(贾镇源), Yu-Han Zhong(钟玉菡), Hua-Yue Mei(梅华悦), Chun-Mei Li(李春梅), and Nan-Pu Cheng(程南璞)†

Faculty of Materials and Energy, Southwest University, Chongqing 400715, *China*

(Received 8 November 2017; revised manuscript received 18 January 2018; published online 26 April 2018)

The hydrostatic-pressure-dependent mechanical stability and optoelectronic behavior of $Zn_4B_6O_{13}$ (ZBO) are calculated using the exchange-correlation functional Perdew–Burke–Ernzerhof generalized gradient approximation and the hybrid functional PBE0 based on density functional theory. The calculated and experimental unit cell volumes and Vickers hardness of ZBO at zero pressure agree well. ZBO is mechanically stable under the critical pressure of 52.98 GPa according to the generalized stability criteria. Furthermore, Young's modulus and Vickers hardness decrease with increasing hydrostatic pressure. The strength and type of ZBO bonds are investigated by population and electron density difference. The electronic structure at zero pressure reveals that ZBO is an indirect band gap semiconductor, and the calculated 5.62-eV bandgap coincides well with the 5.73-eV experimental value, highlighting the success of the hybrid functional PBE0 calculations of electronic properties. The band gap almost increases as a second-order polynomial of pressure, and the indirect nature does not change with the applied external pressure. The optical reflectivity and absorption coefficient show that ZBO is an excellent ultraviolet photodetector. Our calculation results suggest that the elastic and optical properties of ZBO are highly stable over a wide pressure range.

Keywords: $Zn_4B_6O_{13}$ crystal, density functional theory, elastic properties, optical properties

PACS: 71.20.Nr, 71.15.Mb, 62.20.–x, 78.20.–e **DOI:** 10.1088/1674-1056/27/5/057101

1. Introduction

Inorganic borates have attracted considerable attention over the past few decades because of their rich structures and distinctive physical/chemical properties.[1–5] In the crystal structures of inorganic borates, generally, a flat triangular structure can be formed with one boron atom and three oxygen atoms (BO_3), or a tetrahedral-shaped structure can be composed of one boron atom and four oxygen atoms (BO_4), i.e., a boron atom can be sp^2-hybridized with three oxygen atoms or sp^3-hybridized with four oxygen atoms. The common oxygen-atom-linked BO_3 or BO_4 groups can be composed of isolated rings and cages or polymerize into infinite chains, sheets, and networks to form rich borate structures.[1] Plentiful borates have been found, and some have been synthesized and industrialized. For example, iron borate ($FeBO_3$) is a magneto-optical crystal for magnetic storage materials;[2] magnesium borate (MgB_4O_7) is a thermosensitive material;[3] lithium tetraborate ($Li_2B_4O_7$) is a new type of piezoelectric crystal used in mobile communication engineering; and NYAB ($NdAl_3(BO_3)_4$) is an important laser crystal material in the research field of solid-state lasers.[4,5] Rare earth borates are significant host materials for fluorescence because of their high photoluminescence performance and chemical stability. In addition, borate materials like LiB_3O_5,[6] $Sr_2Be_2B_2O_7$,[7] $CsLiB_6O_{10}$,[8] and CsB_3O_5[9] are perfect linear and non-linear optical materials.[10]

Zinc borates have been widely used in many fields, e.g., as polymer additives of flame-retardant synergists, anti-arcing agents, preservatives in wood composites and additives for smoke and afterglow inhibition. In the binary system of ZnO-B_2O_3, at least three compounds have been proposed, including zinc tetraborate (ZnB_4O_7), zinc orthoborate ($Zn_3B_2O_6$) and zinc metaborate (ZBO).[11] The ZBO crystal is special because it is one of the few anhydrous metaborates with all the boron atoms in a fourfold coordination.[12] The qualitative measurements of the photoelastic properties of ZBO performed by Bohaty showed high unexpected effects that suggest an application for acousto-optical deflection devices.[13] Over the past decade, many researchers have shown great interest in UV-irradiation-induced defects in ZBO and found that ZBO is a valuable substrate for afterglow luminescence materials because of its multiple defect centers.[14,15] Recently, Jiang[16] prepared ZBO single crystal via solid-state reaction. The as-received ZBO single crystal was a transparent semiconductor with an optical band gap of 5.73 eV and an important three-dimensional near-zero expansion character. As a result, ZBO has promise for applications in ultraprecise optical instruments often used in the UV region.

The scientific community has no detailed study on the hydrostatic-pressure-dependent mechanical stability and optoelectronic behavior of ZBO. This work aims to conduct a complementary investigation of ZBO under conditions of different hydrostatic pressures with first-principle methods and provides much information regarding the mechanical and op-

*Project supported by the National Natural Science Foundation of China (Grant No. 51171156).

†Corresponding author. E-mail: cheng_np@swu.edu.cn

© 2018 Chinese Physical Society and IOP Publishing Ltd

toelectronic behavior of this important material below a critical pressure.

2. Model structure and computational methods

2.1. Model structure

ZBO crystallizes in a cubic structure within an *I*-43*m* space group forming a $B_{24}O_{48}$ sodalite cage in which the O^1 atom at the center of the unit is surrounded by four ZnO_4 tetrahedra, three BO_4 groups are bonded by one Zn atom via relatively strong Zn–O^2 bonds, and 24 BO_4 tetrahedra are corner-shared by O^2 atoms as shown in Fig. 1.

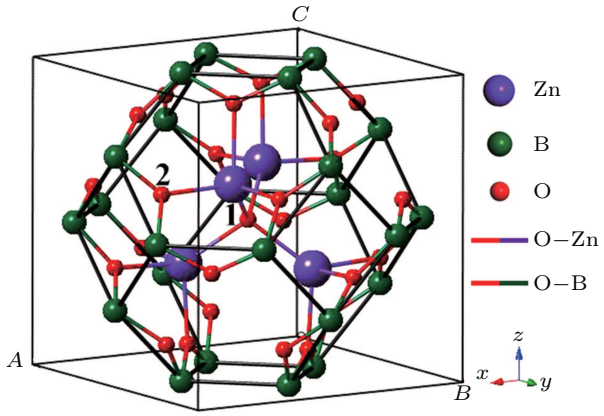


Fig. 1. (color online) ZBO crystal structure.

2.2. Computational methods

The calculations presented in the current work were performed using the Cambridge Serial Total Energy Package code which uses pseudopotentials to depict electron–ion interactions and represents electronic wave functions by using a plane-wave basis set.[17–19] In the calculations of ZBO geometric and mechanical properties and population and electron density differences, the Perdew–Burke–Ernzerhof (PBE) generalized gradient approximation was used for the electron exchange correlation, the ultra-soft pseudopotential was adopted to describe the interactions between the valence electrons and ionic core, and the kinetic energy cutoff of the plane-wave basis set was sufficiently set at 500 eV. Note that, in the current work, the band structures, density of states and optical properties of ZBO were calculated by adopting the hybrid functional PBE0 and the norm-conserving pseudopotential with a kinetic energy cutoff of 750 eV. The hybrid functional PBE0 overcomes the shortcomings of previous band structure calculations of solids performed within generalized gradient approximation and LDA approaches which often significantly underestimate the band gaps in comparison with experimental results.[20] In all calculations, the electrons $Zn3d^{10}4s^2$, $B2s^22p^1$, and $O2s^22p^4$ were treated as valence states. The Monkhorst–Pack[21] scheme k-points grid sampling was set at $8\times8\times8$ points for the first Brillouin zone. All atoms were fully relaxed to their equilibrium positions when the maximum force on each atom was less than 0.01 eV/Å, the total energy change converged to 5.0×10^{-7} eV/atom, the maximum stress on each atom was below 0.02 GPa, and the displacement change of each atom was less than 5.0×10^{-4} Å.

3. Results and discussion

3.1. ZBO mechanical properties

Within the framework of density functional theory calculations, the study of the ZBO crystal structure provides an initial passage to investigate its other physical properties. After geometrical optimization, the ZBO lattice parameters and unit cell volumes at different external hydrostatic pressures less than 50 GPa are shown in Table 1 and Fig. 2. The unstressed lattice parameter is close to the experimental value of 7.47 Å.[16] It is clear that the lattice constant and cell volume decreased with increasing hydrostatic pressure. The equilibrium cell volume V_0 and bulk modulus B_0 at $T = 0$ K are obtained by fitting the Birch–Murnaghan equation of state (EOS)[22]

$$P(V) = \frac{3B_0}{2}\left[\left(\frac{V_0}{V}\right)^{7/3} - \left(\frac{V_0}{V}\right)^{5/3}\right] \times\left\{1+\frac{3}{4}(B_0'-4)\left[\left(\frac{V_0}{V}\right)^{2/3}-1\right]\right\}. \quad (1)$$

The ZBO *P*–*V* relationship is shown in Fig. 2. The cell volume and bulk modulus at 0 K obtained by fitting the Birch–Murnaghan equation are 429.378 $Å^3$ and 181.659 GPa, respectively.

Table 1. ZBO pressure-dependent lattice constants and unit cell volume.

Pressure	a/Å	V/$Å^3$
0 GPa	7.550	430.074
5 GPa	7.480	418.922
10 GPa	7.425	409.299
20 GPa	7.321	392.352
30 GPa	7.234	378.592
40 GPa	7.159	366.930
50 GPa	7.092	356.728

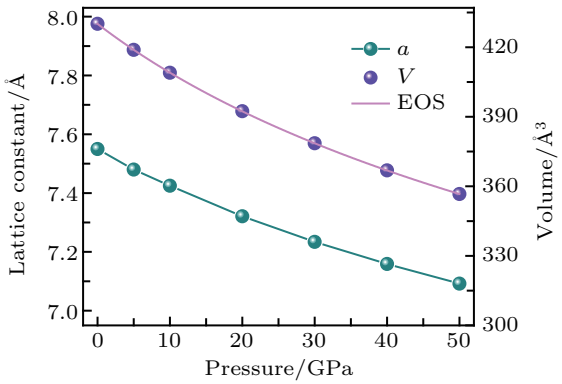


Fig. 2. (color online) ZBO pressure-dependent lattice constants and unit cell volumes.

ZBO has only three independent elastic constants, namely, C_{11}, C_{12} and C_{44} because of its cubic structure with space group I-43m. The elastic constant C_{11} represents the resistances to linear compression in the x, y and z directions, and a longitudinal strain induces a change in C_{11}. The elastic constants C_{12} and C_{44} representing the elasticity in shape are shear constants. The calculated elastic constants C_{ij} of ZBO at different hydrostatic pressures are shown in Table 2. We present the variations of C_{11}, C_{12} and C_{44} with respect to the applied external pressure in Fig. 3. At zero pressure, C_{11} is the highest of the elastic constants, implying that ZBO is not easily compressed along the principal axes. All elastic constants are nearly linearly dependent on pressure in the considered range, especially below 10 GPa. Simultaneously, C_{11} and C_{12} increase quickly and C_{44} decreases slowly with increasing pressure, meaning that C_{11} and C_{12} are more sensitive to the external applied pressure than C_{44}. This phenomenon may be the result of the ZBO sodalite cage structure.

Table 2. Pressure-dependent elastic constants C_{ij} (in GPa).

C_{ij}	0 GPa	5 GPa	10 GPa	20 GPa	30 GPa	40 GPa	50 GPa
C_{11}	287.844	305.488	324.532	352.317	376.442	399.519	417.363
C_{12}	122.883	144.700	169.202	214.845	260.664	307.391	354.237
C_{44}	96.436	96.300	95.913	93.488	88.562	83.435	76.939

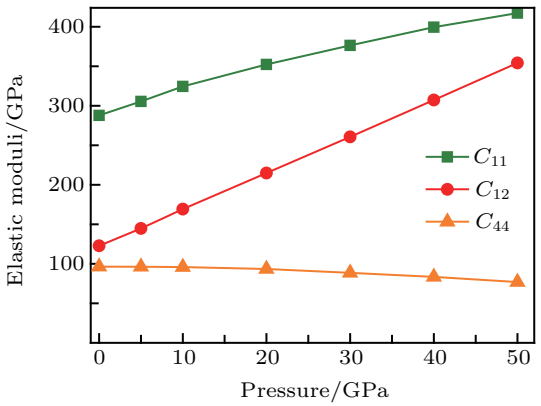


Fig. 3. (color online) Elastic moduli C_{11}, C_{12} and C_{44} as functions of pressure.

To ensure that ZBO is stable at a given hydrostatic pressure, the three independent elastic constants must match the generalized elastic stability criteria[23] listed below

$$\widetilde{C_{11}} = C_{11}, \tag{2}$$

$$\widetilde{C_{12}} = C_{12} + P, \tag{3}$$

$$\widetilde{C_{44}} = C_{44} - 0.5P, \tag{4}$$

$$M_1 = \widetilde{C_{11}} + 2\widetilde{C_{12}} > 0, \tag{5}$$

$$M_2 = \widetilde{C_{11}} - \widetilde{C_{12}} > 0, \tag{6}$$

$$M_3 = \widetilde{C_{44}} > 0, \tag{7}$$

where P is an extra applied hydrostatic pressure. The values of the generalized stability coefficient M_i as a function of the applied hydrostatic pressure are shown in Table 3 and Fig. 4. From Fig. 4, M_1 is positive at zero pressure and increases with an increase of pressure, meaning that M_1 always satisfies the criteria. However, since M_2 and M_3 monotonically decrease in the pressure range 0–50 GPa and may not meet the criteria when pressure is beyond 50 GPa, polynomial least square fittings were performed for M_2 and M_3. The adjusted determination coefficients of M_2 and M_3 fittings were 0.9996 and 0.9997, respectively. It can be predicted that M_2 becomes negative when pressure is greater than 52.98 GPa, indicating that the material will keep its mechanical stability below this critical pressure and that there is no structural phase transition from 0 to 52.98 GPa.

Table 3. Pressure-dependent M_i (in GPa) for ZBO.

M_i	0 GPa	5 GPa	10 GPa	20 GPa	30 GPa	40 GPa	50 GPa
M_1	533.061	604.888	672.936	802.006	927.770	1054.300	1175.837
M_2	164.961	155.788	145.330	117.472	85.778	52.128	13.126
M_3	96.436	93.800	90.713	83.488	73.561	63.435	51.939

Based on elastic constants, Voigt and Reuss approximations[24] are widely used to calculate the bulk modulus B and the shear modulus G of solids. The bulk modulus B reflects the ability of solids to defend compression, while the shear modulus G stands for the ability of solids to defend shear deformation. For a cubic system, the Voigt and Reuss approximations of B and G can be obtained by

$$B_{\mathrm{V}} = B_{\mathrm{R}} = (C_{11} + 2C_{12})/3, \tag{8}$$

$$G_{\mathrm{V}} = (C_{11} - C_{12} + 3C_{44})/5, \tag{9}$$

$$G_{\mathrm{R}} = 5\,(C_{11} - C_{12})\,C_{44}/[4C_{44} + 3(C_{11} - C_{12})]. \tag{10}$$

Hill[25] confirmed that the Voigt and Reuss models represent the extreme upper and lower bounds, respectively, and the arithmetic average value VRH (Voigt–Reuss–Hill) is close to the experimental results. The arithmetic average values of B and G can be written as

$$B = (B_{\mathrm{V}} + B_{\mathrm{R}})/2, \tag{11}$$

$$G = (G_V + G_R)/2. \quad (12)$$

The calculated arithmetic average values of bulk modulus B and shear modulus G of ZBO are summarized in Table 4. The bulk modulus B obtained from Eq. (11) shown in Table 4 matches well with that obtained from the Birch–Murnaghan equation of state at zero pressure, indicating that our calculation is self-affirming and reliable. At zero pressure, the ZBO bulk modulus was 177.87 GPa, which is larger than the predicted value of α-ZnB_4O_7 by Winkler,[26] indicating that ZBO may have greater mechanical strength than that of α-ZnB_4O_7. The ZBO bulk modulus increases with the increase in pressure, whereas the shear modulus decreases, i.e., the ability to resist compression was enhanced while the ability to resist shear deformation was weakened. For a cubic system, the shear modulus for the $\{100\}$ plane along the [010] direction is given by $G\{100\} = C_{44}$, and the shear modulus for the $\{110\}$ plane along the $[1\bar{1}0]$ direction is represented by $G\{110\} = (C_{11} - C_{12})/2$. As shown in Table 4, in the pressure range 0–50 GPa, the ZBO shear modulus $G\{100\}$ was always greater than $G\{110\}$, showing that ZBO is more difficult to shear on the $\{100\}$ plane in the [010] direction than on the $\{110\}$ plane in the $[1\bar{1}0]$ direction.

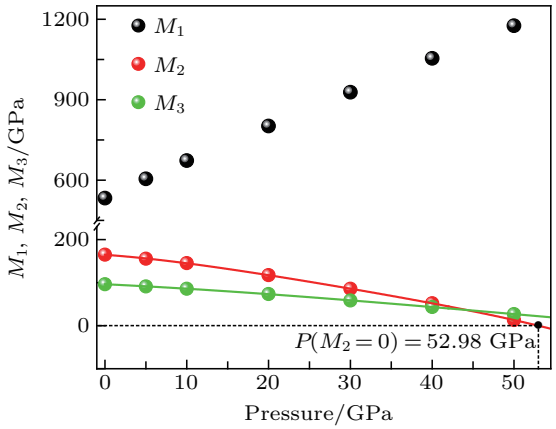


Fig. 4. (color online) M_1, M_2 and M_3 for ZBO as function of hydrostatic pressure.

Based on the calculated B and G above, Pugh's ratio B/G, Poisson's ratio γ, Vickers hardness H_v, Young's modulus E and anisotropic index A^U can be obtained[27–30]

$$\gamma = \frac{3B - 2G}{2(3B + G)}, \quad (13)$$

$$H_v = 1.887\left[\left(\frac{G}{B}\right)^2 G\right]^{0.585}, \quad (14)$$

$$E = \frac{9BG}{3B + G}, \quad (15)$$

$$A^U = 5\frac{G_V}{G_R} + \frac{B_V}{B_R} - 6. \quad (16)$$

Pugh's ratio B/G[27] describes the ductile or brittle behavior of solids. A high B/G ratio means that the ductility of a solid is high. If $B/G > 1.75$, the material exhibits ductility, otherwise the material is brittle. In Table 4, at zero pressure, the ZBO B/G ratio is 1.964, revealing that ZBO is weakly ductile. It also shows that the B/G ratio increases when the applied pressure increases, meaning that ZBO is ductile in nature in the entire pressure range. Poisson's ratio γ,[28] another useful index, is indicative of the degree of covalent bond directionality. The lower and upper limits of γ are 0.25 and 0.50, respectively, for central forces in solids. At zero pressure, the ZBO Poisson's ratio is greater than the lower limit (0.25), revealing that the ZBO interatomic forces are central forces.[31] The Poisson's ratio can also be used to predict the brittleness or ductility of solids. In other words, the Pugh's ratio and the Poisson's ratio can represent the similar intrinsic attributes of solids. For a compound, if $\gamma < 0.26$, it is brittle; otherwise, it is ductile.[32] As the applied hydrostatic pressure increases, the γ of ZBO also increases. Consequently, there is a similar trend between the pressure dependent B/G and γ of ZBO (see Table 4).

The Vickers hardness H_v often described by an empirical formula is a very important property used to measure the hardness of solids.[29] The obtained theoretical Vickers hardness of ZBO at zero pressure was 11.96 GPa, which is close to the experimental value of 1304 kg/mm^2 (namely, 12.37 GPa),[16] confirming that ZBO has high mechanical strength. However, as shown in Table 4, the hardness of ZBO decreases as the external pressure increases because of the dominant role of the decreased shear modulus.

The Young's modulus E represents the ratio of a simple tensile stress to a corresponding tensile strain and is calculated by Eq. (15); it is usually used to estimate the stiffness of materials. The larger the Young's modulus, the stiffer the material. The Young's modulus of ZBO slightly increased in the pressure range 0–5 GPa and decreased when the applied pressure was greater than 5 GPa. From Young's modulus $E = 9BG/(G+3B)$[28] and the results of Table 4, we know that the competition between the increased bulk modulus B and the decreased shear modulus G caused a nonlinear variation of the Young's modulus. When the applied external pressure was within 5 GPa, the bulk modulus was weakly dominant. However, the shear modulus played the leading role when the applied external pressure was greater than 5 GPa. The Young's modulus of ZBO tends to decrease with increasing pressure.

The directional dependence of Young's modulus of ZBO is illustrated in Fig. 5. Figure 5(a) shows the weak anisotropy of ZBO at zero pressure. From Figs. 5(b)–5(g), we know that when a hydrostatic pressure is applied, Young's modulus of ZBO becomes smaller while the degree of anisotropy becomes larger. Since ZBO belongs to the cubic system, Young's modulus projections on the $\{001\}$, $\{010\}$ and $\{100\}$ planes are exactly the same (see Figs. 5(a)–5(g)), therefore, only the projection of the $\{001\}$ plane is presented in Fig. 5(h). It is obvious that Young's modulus is nearly unchanged when the applied external pressure is less than 10 GPa, i.e., Young's modulus of ZBO is weakly dependent on pressure, i.e., ZBO is quite stable under low external pressures.

Table 4. B (in GPa), G (in GPa), E (in GPa), γ, H_v (in GPa), B/G and A^U of ZBO.

Pressure	B	G_V	G_R	G	$G\{110\}$	B/G	γ	H_v	E	A^U
0	177.87	90.85	90.32	90.59	82.48	1.96	0.282	11.960	232.32	0.030
5	198.30	89.94	89.24	89.59	80.39	2.21	0.304	10.330	233.59	0.039
10	220.98	88.61	87.67	87.14	77.67	2.51	0.324	8.845	233.40	0.054
20	260.67	83.59	81.72	82.65	68.74	3.15	0.357	6.512	224.26	0.114
30	299.26	76.29	73.08	74.68	57.89	4.00	0.385	4.640	206.84	0.220
40	338.10	68.49	62.99	65.74	46.06	5.14	0.409	3.214	185.22	0.436
50	375.28	58.79	48.85	53.82	31.56	6.97	0.432	2.002	154.09	1.017

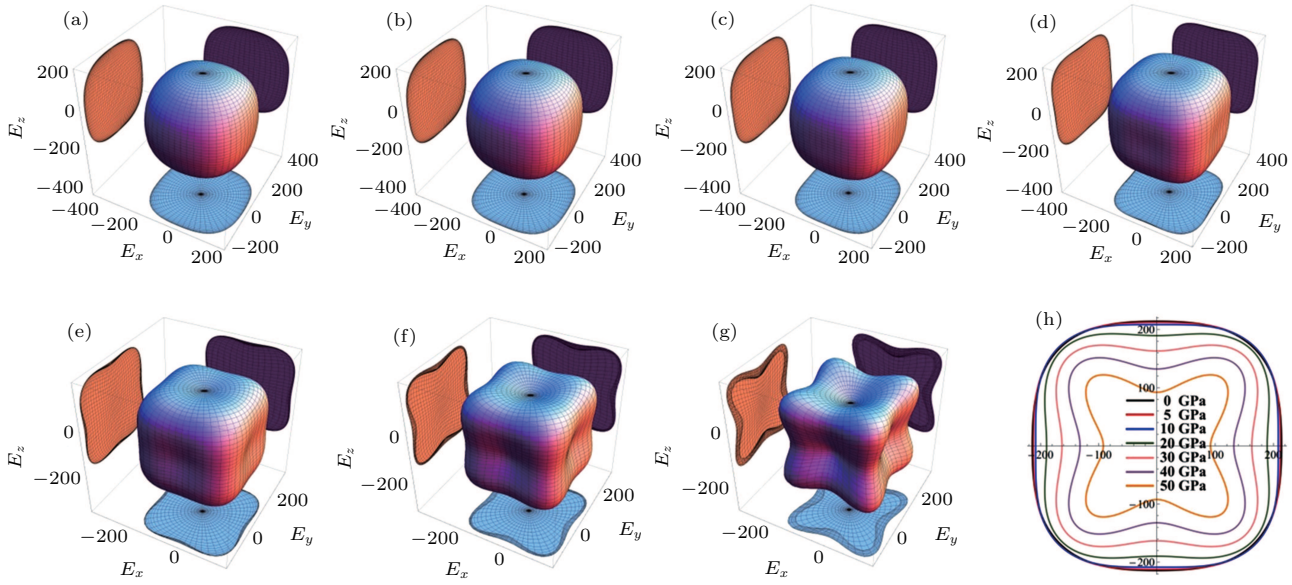


Fig. 5. (color online) Directional dependence of the Young's modulus of ZBO: (a) 0 GPa, (b) 5 GPa, (c) 10 GPa, (d) 20 GPa, (e) 30 GPa, (f) 40 GPa, and (g) 50 GPa.

The universal elastic anisotropy index A^U for all crystal phases introduced by Ranganathan[30] is often used to quantitatively study monocrystalline anisotropy. For a completely isotropic material, the elastic anisotropy factor A^U is equal to 0, while any value larger than 0 indicates anisotropy. The higher the value, the higher the degree of anisotropy. The anisotropy values shown in Table 4 indicate that ZBO exhibits a weak anisotropy at zero pressure. With an increase in pressure, the anisotropy index increases slowly, which is consistent with the pressure-dependent Young's modulus (see Fig. 5).

3.2. Electronic structures

3.2.1. Population and electron density difference

To investigate the stress effects on the bonds in ZBO, we present only the bond lengths, bond populations and electron density differences for 0 and 50 GPa in Table 5 and in Fig. 6. Compared with the experimental data at 13 K,[16] the lengths of Zn–O^1, Zn–O^2 and B–O^2 bonds at 0 GPa have relative errors of 1.2%, 1.7%, and 0.68%, respectively, indicating the calculated values agree well with the experimental data. At zero pressure, the bond populations of B–B and Zn–B bonds are negative, meaning that both are antibonding states.[33] However, the bond populations of Zn–O^1, Zn–O^2 and B–O^2 are positive and increase with an increase in the external pressure; that is, all the bonds have covalent characteristics and become stronger as the pressure increases and the B–O^2 bonds are the strongest. Even when an external pressure of 50 GPa is applied, the compression rates of Zn–O^1, Zn–O^2 and B–O^2 bonds are merely 9.7%, 6.7% and 4.6%, respectively, confirming that ZBO has strong mechanical strength.

From the electron density differences of ZBO in Figs. 6(a) and 6(b), we can see that Zn–O^1 and Zn–O^2 are covalent with partial ionic characteristics,[34] and the directivity of accumulated electrons between the B and O^2 atoms reveals that B–O^2 bonds have strong covalent characteristics. In Figs. 6(c) and 6(d), when an external pressure of 50 GPa was applied, the overlap degree of the electron cloud between the covalent bonds increased, leading to the enhancement of covalent characteristics.

Table 5. ZBO bond lengths and bond populations.

	Experimental	0 GPa		50 GPa	
	length	length	population	length	population
Zn–O_1	1.985	2.008	0.33	1.814	0.38
Zn–O_2	1.959	1.993	0.36	1.860	0.43
B–O_2	1.475	1.485	0.66	1.417	0.70
B–B		2.671	–0.12	2.509	–0.13
Zn–B		2.954	–0.18	2.807	–0.23

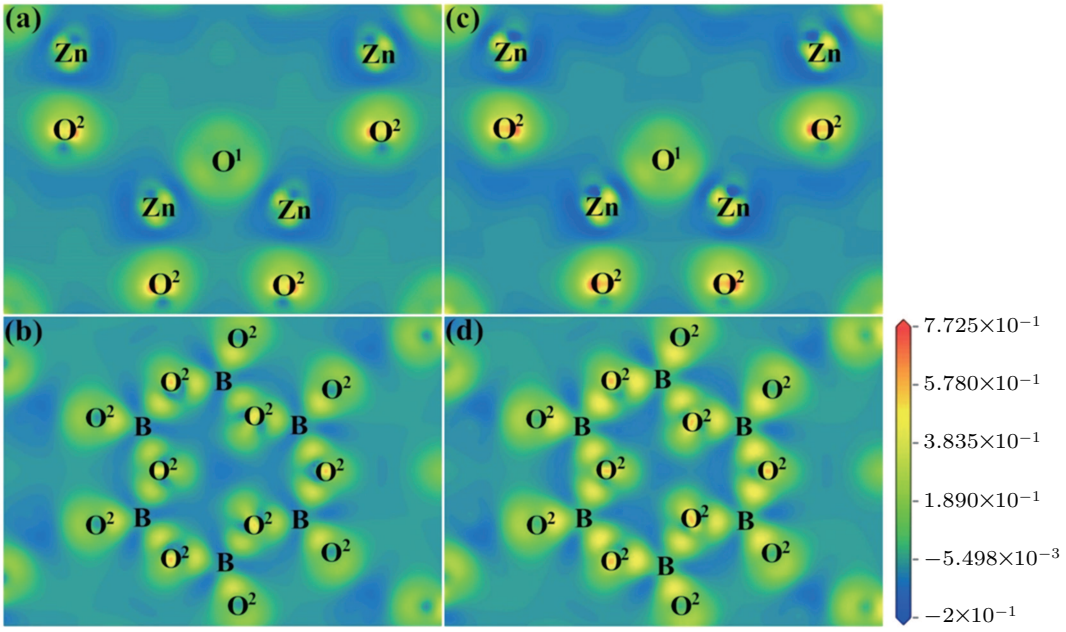


Fig. 6. (color online) ZBO electron density differences: (a) {110} plane and (b) {111} plane for 0 GPa and (c) {110} and (d) {111} plane for 50 GPa.

3.2.2. Density of states and band structures

After confirming the mechanical stability of ZBO under hydrostatic pressures less than 52.98 GPa, we used the hybrid functional PBE0 to investigate its density of states and band structures within the same pressure range. According to the total and partial density of states of ZBO at zero pressure displayed in Fig. 7, the energy bands can be divided into three groups. The Fermi energy level was set at the top of the valence band. The lowest group had significant contributions from the O-2s states around −19.10 eV. The second group from −10 eV to the Fermi level can be further divided into two parts. The first part located in −10 to −4 eV were occupied mostly by Zn-3d states with slight contributions from the O-2p and B-2p states; in the second part from −4 eV to the Fermi level, the O-2p states were the most dominant while Zn-3d states were observed. The Zn-4s states contributed to the bottom of the conduction bands. Note that there were tails at the Fermi level because of Gaussian smearing, but the semiconducting nature was reproduced successfully.[35]

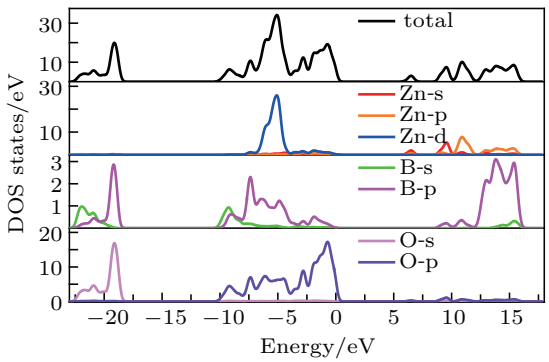


Fig. 7. (color online) Total and partial density of ZBO states at zero pressure.

Figure 8 displays the band gaps and density of states of ZBO at different pressures less than 50 GPa. In Fig. 8(a), at zero pressure, the theoretical ZBO band gap of 5.62 eV calculated by PBE0 was close to the experimental optical band gap of 5.73 eV,[16] which emphasizes the success of the hybrid functional PBE0 during calculations of the electronic properties of ZBO. Compared with the band gap of β-$Zn_3B_2O_6$ (3.26 eV),[36] ZBO is more adaptable for applications in the short-wave UV light energy range. In addition, ZBO nanocrystals synthesized by Alemi[37] showed a band gap of 3.306 eV, which may inspire us to broaden optical applications by adjusting the ZBO band gap values. Obviously, the maximum of the valence band for each pressure is at the symmetry point N in the first Brillouin zone, while the minimum of the conduction band is at the symmetry point G, revealing that ZBO is always an indirect bandgap semiconductor and will not change with pressure. In other words, for ZBO, the applied external pressures will not cause a transformation from an indirect to a direct band gap. The total density of states of ZBO at different pressures presented in Fig. 8(b) shows that the conduction bands move to the high energy zone with increasing pressure, which is consistent with the band structures shown in Fig. 8(a). This phenomenon happens because the increasing pressure drives the hybridized orbitals between O-2p and Zn-3d to a higher degree, meaning that the Zn–O bonds will be shorter and stronger. This can effectively decrease the energies of valence bands and thus expand the band gap.[16] As a result, the ZBO band gap increases with increasing pressure.

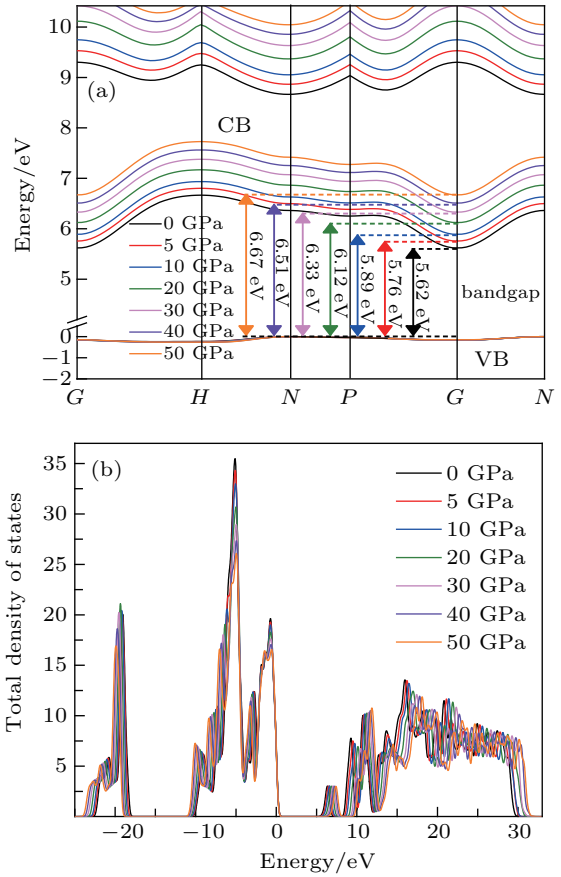


Fig. 8. (color online) Pressure-dependent band gaps and total density of ZBO states.

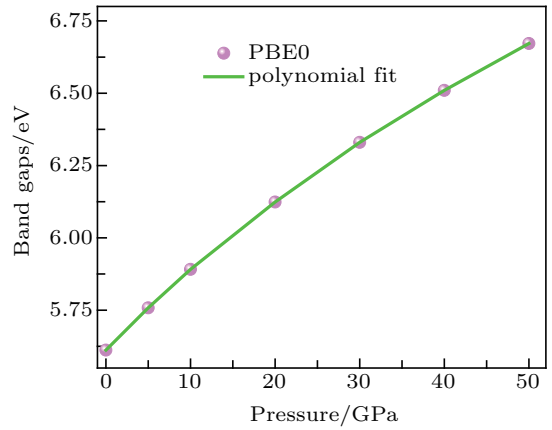


Fig. 9. (color online) Band gaps as a function of ZBO hydrostatic pressure.

Considering that energy band gaps of solids can be described as a function of pressure, this variation can be described as

$$E_g(P) = E_g(0) + \alpha P + \beta P^2, \tag{17}$$

where $E_g(P)$ and $E_g(0)$ represent the band gap energies calculated at a given pressure P and at $P = 0$ GPa, respectively. α is the linear pressure coefficient and β is the quadratic pressure coefficient. The polynomial fitting of the pressure-dependent band gaps is plotted in Fig. 9. Within the mechanical stability pressure range, the constant term $E_g(0)$ for ZBO is 5.62 eV (consistent with the ZBO band gap at zero pressure), the linear pressure coefficient is 0.028 eV·GPa^{-1}, the quadratic pressure coefficient is -1.414×10^{-4} eV·GPa^{-2} and the adjusted determination coefficient is 0.9998. In terms of the small linear and quadratic pressure coefficients, we conclude that the ZBO band gap is stable and slightly dependent on pressure.

3.3. Optical properties

During the ZBO optical property calculations, 216 empty bands (three times the number of occupied bands) were adopted to consider as many electron transitions as possible.

The study of radiation–matter interaction causing electronic transitions is essential to investigate the optical behavior of ZBO. This interaction can be described by the well-known complex dielectric function $\varepsilon(\omega)$[38]

$$\varepsilon(\omega) = \varepsilon_1(\omega) + \mathrm{i}\varepsilon_2(\omega). \tag{18}$$

The imaginary part $\varepsilon_2(\omega)$ is given by

$$\varepsilon_2(\omega) = \frac{4\pi^2 e^2}{Vm^2\omega^2} \sum_{nn'} \int \mathrm{d}^3\boldsymbol{k} |\langle \boldsymbol{kn}|p|\boldsymbol{kn}'\rangle|^2 \times |f(\boldsymbol{kn})[1 - f(\boldsymbol{kn}')]\delta(E_{\boldsymbol{kn}} - E_{\boldsymbol{kn}'} - \hbar\omega), \tag{19}$$

where e, m and V denote the charge, mass and unit cell volume of free electrons, respectively, and ω is the frequency of the incident photons. p and $\boldsymbol{kn}$ represent the momentum operator in the bracket notation and the wave function with crystal momentum $\boldsymbol{k}$, respectively. $f(\boldsymbol{kn})$ is the Fermi–Dirac distribution function which ensures the count of the transitions from occupied to unoccupied states and the condition for the conservation of total energy is represented by $\delta(E_{\boldsymbol{kn}} - E_{\boldsymbol{kn}'} - \hbar\omega)$.

From the imaginary part $\varepsilon_2(\omega)$, the real part $\varepsilon_1(\omega)$ of the dielectric function is obtained from the Kramers–Kronig transformation

$$\varepsilon_1(\omega) = 1 + \frac{2}{\pi} M \int_0^\infty \frac{\omega' \varepsilon_2(\omega')\mathrm{d}\omega'}{\omega'^2 - \omega^2}, \tag{20}$$

where M represents the principal value of the integral. Given that the real and imaginary parts of the frequency-dependent dielectric function are known, one can calculate other important optical properties, such as the absorption coefficient $\alpha(\omega)$, reflectivity $R(\omega)$, refractive index $n(\omega)$, loss function $L(\omega)$, and conductivity $\sigma(\omega)$[39,40]

$$\alpha(\omega) = \sqrt{2}\omega \left[\sqrt{\varepsilon_1^2(\omega) + \varepsilon_2^2(\omega)} - \varepsilon_1(\omega)\right]^{1/2}, \tag{21}$$

$$R(\omega) = \frac{(n(\omega) - 1)^2 + k^2(\omega)}{(n(\omega) + 1)^2 + k^2(\omega)}, \tag{22}$$

$$n(\omega) = \frac{1}{\sqrt{2}} \left[\sqrt{\varepsilon_1(\omega)^2 + \varepsilon_2(\omega)^2} + \varepsilon_1(\omega)\right]^{1/2}, \tag{23}$$

$$L(\omega) = \frac{\varepsilon_2(\omega)}{\varepsilon_1^2(\omega) + \varepsilon_2^2(\omega)}, \tag{24}$$

$$\sigma(\omega) = \frac{\omega\varepsilon_2(\omega)}{4\pi}. \tag{25}$$

Figure 10 shows the imaginary and real parts of the ZBO dielectric function in the energy range 0–35 eV. We can see that at zero pressure, the imaginary part $\varepsilon_2(\omega)$ for ZBO has peaks at 7.17, 12.39 and 15.70 eV. Peak A located at 7.17 eV corresponds mainly to the transitions from the top of the valence bands formed by the hybridized orbitals between O-2p and Zn-3d to the bottom of the conduction bands formed by the empty Zn-4s orbitals. Peak B corresponds to the transitions from the hybridized orbitals between O-2p and Zn-3d to the empty Zn-4s and Zn-3p. Peak C corresponds to the transitions from the hybridized orbitals between O-2p and Zn-3d to the empty Zn-4s, 3p and B-2p states. With increasing external pressure, $\varepsilon_2(\omega)$ is almost the same, except that there is a small shift toward higher energies (blue shift), which is consistent with the conclusion drawn from the band structure and density of states: the applied external pressure can expand the ZBO band gap. As shown in Fig. 10, one can see that the $\varepsilon_1(\omega)$ of ZBO has a series of peaks from 0 to 20 eV and exhibits good dielectric performance. The ZBO static dielectric constant displayed in Fig. 11 shows that $\varepsilon_0(P)$ increases monotonically with increasing pressure and can be described through a quadratic polynomial (namely, $\varepsilon_0(P) = 2.344 + 0.0013P - 3.28 \times 10^{-6}P^2$) within the mechanical stability range. The external pressure had hardly any impact on the static dielectric constant, indicating that ZBO has stable optical properties.

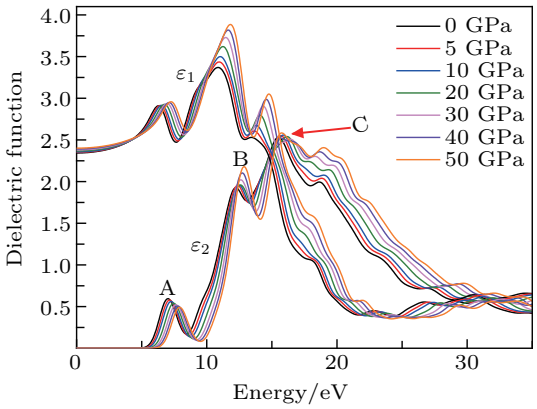


Fig. 10. (color online) Imaginary and real parts of pressure-dependent ZBO dielectric functions.

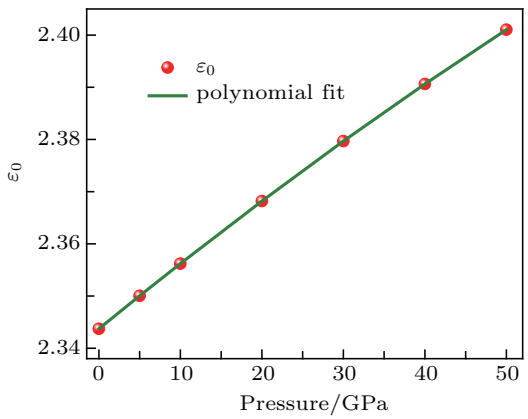


Fig. 11. (color online) Static dielectric constant as a function of pressure.

The absorption coefficient $\alpha(\omega)$, refractive index $n(\omega)$, loss function $L(\omega)$ and conductivity $\sigma(\omega)$ of ZBO at different pressures are plotted in Fig. 12. As can be seen from Fig. 12(a), the ZBO absorption coefficient is almost zero in the visible range, whereas it is prominent in the UV range. At zero pressure, the calculated optical absorption edge was 5.30 eV, which was close to the calculated band gap. The peaks of the absorption coefficient corresponded to those of the imaginary part of the dielectric function shown in Fig. 10. The absorption coefficient $\alpha(\omega)$ was blue shifted along with $\varepsilon_2(\omega)$ because of the compression. At zero pressure, the maximum reflectivity $R(\omega)$ was 13.5% at 15.7 eV in the UV spectra, and the reflection range was blue shifted as the external pressure increased. It is worth noting that ZBO is a perfect UV photodetector because of its low reflectivity and high absorption coefficient in the UV region. From $n_0^2 = \varepsilon_0$, the static refractive index was 1.53 at zero pressure, higher than the static refractive index of β-$Zn_3B_2O_6$,[36] and the applied external pressure caused the refractive index to increase slightly. The refractive index $n(\omega)$ reached a peak around 11.08 eV at zero pressure and was blue shifted when the hydrostatic pressure was applied. The electron energy-loss function $L(\omega)$ displayed in Fig. 12(c) is an important optical function often used to describe the energy loss of a fast electron passing through a material. In addition, the peaks of $L(\omega)$ correspond to the trailing edges in the reflection spectra. For instance, the peaks of $L(\omega)$ for ZBO at zero pressure were at 24.93, 27.90 and 31.70 eV corresponding to the abrupt reduction of $R(\omega)$. The peaks represent the characteristic behaviors associated with the plasma oscillations, and the corresponding frequencies are the so-called plasma frequencies.[41] The main peak of $L(\omega)$ for ZBO at zero pressure was at 24.93 eV and was blue shifted as the external pressure increased. The conductivity $\sigma(\omega)$ reflects the effect of different photon energies on the conductivity of solids. According to Fig. 12(d), the ZBO conductivity $\sigma(\omega)$ was zero when the photon energy was within the visible light energy range because there were no free electrons beyond the Fermi level under this circumstance. However, high-energy UV photons have a great impact on the conductivity of ZBO. The conductivity of ZBO increases and drifts toward a high energy zone as the external pressure increases. The transmittance spectra[42] of solids can be easily obtained by utilizing the relation

$$T(\omega) = \frac{[1-R(\omega)]^2 e^{-\alpha(\omega)t}}{1-R(\omega)^2 e^{-2\alpha(\omega)t}}, \tag{26}$$

where $\alpha(\omega)$ and $R(\omega)$ are the absorption coefficient and the reflectivity, respectively, and t is the sample thickness. The ZBO transmittance spectra with different sample thicknesses at zero pressure are plotted in Fig. 13. When the sample thickness was 40 mm, the transmittance spectrum provided a simi-

lar trend between our results and the experimental results.[16] Note the transmittance peaks around 140 nm when the sample thickness was less than 0.5 μm caused by the minimum absorption coefficient around 140 nm (i.e., 8.89 eV) shown in Fig. 12(a). However, the increased sample thickness weakens the impact of the absorption coefficient on transmittance. As a result, the peak decreases as the thickness increases and eventually disappears. The transmittance is thickness-dependent when the photon wavelength is within 300 nm. Also, the thinner the sample, the higher the transmittance. However, when the photon wavelength is greater than 300 nm, the nearly zero absorption coefficient causes high transmittance. Thus, one can see that ZBO is transparent within the long-wave UV light and the visible light energy ranges and that transmittance is thickness-independent at this time.

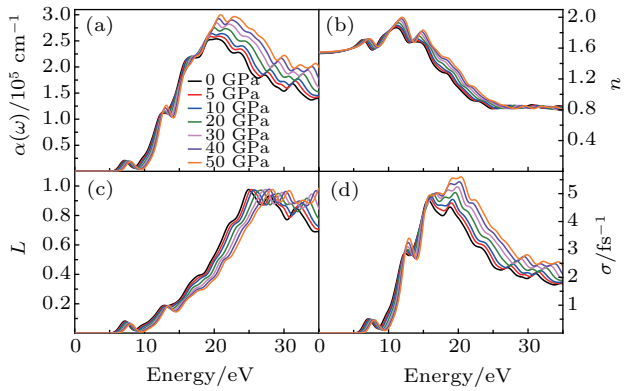


Fig. 12. (color online) Pressure-dependent ZBO optical properties: (a) absorption coefficient $\alpha(\omega)$, (b) refractive index $n(\omega)$, (c) loss function $L(\omega)$, and (d) conductivity $\sigma(\omega)$.

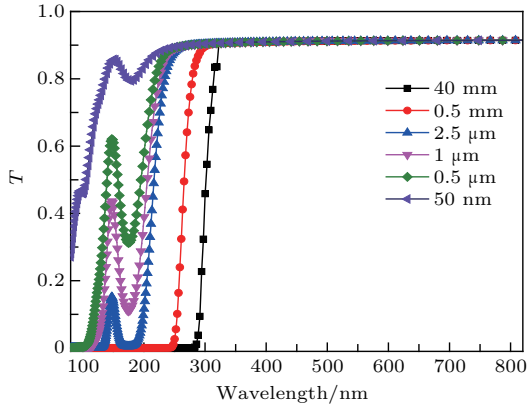


Fig. 13. (color online) ZBO transmittance at zero pressure.

4. Conclusion

The current work provides a theoretical prediction of the effect of hydrostatic pressure on the mechanical properties and optoelectronic behavior of ZBO crystal in the mechanical stability range 0–52.98 GPa. The obtained structural parameters and Vickers hardness were consistent with the observed experimental results. ZBO has high mechanical strength, high Young's modulus and weak anisotropy, and all of these mechanical properties are slightly dependent on external pressure. The B–O^2 bonds are strongest in ZBO while the Zn–O^1 and Zn–O^2 bonds are covalent with ionic characteristics. The top valence bands of ZBO are dominated by O-2p and Zn-3d states, while the conduction bands consist of Zn-4s states. The band gap of ZBO increases as a function of pressure (i.e., $E_g(P) = 5.62 + 0.028P - 1.414 \times 10^{-4}P^2$) within the mechanical stability range because applied external pressure strengthens the hybridization of O-2p and Zn-3d orbitals, which induces an energy decrease of the valence bands and thus expands the energy band gap. The dielectric function of ZBO at hydrostatic pressures has been calculated in a wide energy range. The peaks of the imaginary part of the dielectric function near 7.17, 12.39 and 15.70 eV correspond to the transitions from the hybridized orbitals between the O-2p and Zn-3d states to the Zn-4s state, the empty Zn-4s and Zn-3p states, and the empty Zn-4s, Zn-3p, and B-2p states, respectively. ZBO can be a UV photodetector because of its low reflectivity and high absorption coefficient in the UV region. ZBO is transparent within the long-wave UV light and visible light energy ranges in concert with the experiment. In addition, with increasing external pressure, the optical properties of ZBO have a slight blue shift. Both the elastic and optical properties of ZBO are weakly dependent on pressure; therefore, ZBO is stable and adaptive to a wide variety of environments.

References

[1] Chen X, Zhao Y, Chang X, Zuo J, Zang H and Xiao W 2006 *J. Solid State Chem.* **179** 3911
[2] Kirilyuk A, Kimel A V and Rasing T 2010 *Rev. Mod. Phys.* **82** 2731
[3] Lochab S P, Pandey A, Sahare P D, Chauhan R S, Salah N and Ranjan R 2007 *Phys. Status Solid.* **204** 2416
[4] Yang M, Liu L and Chen F 2012 *Mater. Lett.* **88** 116
[5] Tulek A, Polson R C and Vardeny Z V 2010 *Nat. Phys.* **6** 303
[6] Ferrari A C, Bonaccorso F, Fal'Ko V, *et al.* 2015 *Nanoscale* **7** 4598
[7] Wang S, Ye N, Li W and Zhao D 2010 *J. Am. Chem. Soc.* **132** 8779
[8] Han S J, Wang Y, Pan S L, Dong X Y, Wu H P, Han J, Yang Y, Yu H W and Bai C Y 2014 *Cryst. Growth Des.* **14** 1794
[9] Wang Y and Pan S 2016 *Coord. Chem. Rev.* **323** 15
[10] Chen C, Lin Z and Wang Z S 2005 *Appl. Phys. B* **80** 1
[11] Chen X, Xue H, Chang X, Zhang L, Zhao Y, Zuo J, Zang H and Xiao W 2006 *J. Alloys Compd.* **425** 96
[12] Murray A F and Lockwood D J 1976 *J. Phys. C: Solid State Phys.* **9** 3691
[13] Bohatý L, Ochrombel R, Liebertz J and Becker P 2017 *Cryst. Res. Technol.* **52** 1600250
[14] Meijerink A, Blasse G and Glasbeek M 1990 *J. Phys.: Condens. Matter* **2** 6303
[15] Liang P, Wang M Z and Liu Z H 2017 *J. Rare Earths* **35** 441
[16] Jiang X X, Molokeev M S, Gong P F, Yang Y, Wang W, Wang S H, Wu S F, Wang Y X, Huang R J, Li L F, Wu Y C, Xing X R and Lin Z S 2016 *Adv. Mater.* **28** 7936
[17] Štich I, Payne M C, King-Smith R D, Lin J S and Clarke L 1992 *J. Phys. Rev. Lett.* **68** 1351
[18] Hohenberg P and Kohn W 1964 *Phys Rev.* **136** B864
[19] Vanderbilt D 1990 *Phys. Rev. B* **41** 7892
[20] Yelisseyev A, Liang F, Isaenko L, Lobanov S, Goloshumova A and Lin Z S 2017 *Opt. Mater.* **72** 795
[21] Monkhorst H J and Pack J D 1976 *Phys. Rev. B* **13** 5188

[22] Liang H, Peng F, Fan C, Zhang Q, Liu J and Guan S X 2017 *Chin. Phys. B* **26** 053101
[23] Wang J, Yip S, Phillpot S R and Wolf D 1993 *Phys. Rev. Lett.* **71** 4182
[24] Wu Z, Zhao E, Xiang H P, Hao X F, Liu X J and Meng J 2007 *Phys. Rev. B.* **76** 054115
[25] Hill R 1952 *Proc. Phys. Soc. A* **65** 349
[26] Winkler B, Guzman A C, Wiehl L, Bayarjargal L and Milman V 2012 *Solid State Sci.* **14** 1080
[27] Yoo M H 1981 *Metall. Trans. A* **12** 409
[28] Shakil M, Zafar M, Ahmed S, Choudhary M A and Iqbal T 2016 *Chin. Phys. B* **25** 076104
[29] Chen X Q, Niu H, Li D and Li Y 2011 *Intermetallics* **19** 1275
[30] Ranganathan S I and Ostoja-Starzewski M 2008 *Phys. Rev. Lett.* **101** 055504
[31] Pfrommer B G, Côté M, Louie S G and Cohen M L 1997 *J. Comput. Phys.* **131** 233
[32] Vaitheeswaran G, Kanchana V, Svane A and Delin A 2007 *J. Phys.: Condens. Matter* **19** 326214
[33] Ma X, Lu B, Li D, Shi R, Pan C and Zhu Y 2011 *J. Phys. Chem. C* **115** 4680
[34] Zhang F C, Zhang Z Y, Zhang W H, Yan J F and Yun J N 2008 *Chin. Phys. Lett.* **25** 3735
[35] Ming X, Wang C Z, Fan H G, Hu F, Wei Y J, Huang Z F, Meng X and Chen G 2008 *J. Phys.: Condens. Matter* **20** 395204
[36] Chen D G, Cheng W D, Wu D S, Zhang H, Zhang Y C, Gong Y J and Kan Z G 2005 *Solid State Sci.* **7** 179
[37] Alemi A, Mohseni N, Dolatyari M and Bakhtiari A 2012 *Int. J. Bio-Inorg. Hybd. Nanomat.* **1** 79
[38] Smith N V 1971 *Phys. Rev. B* **3** 1862
[39] Yun J N and Zhang Z Y 2009 *Chin. Phys. B.* **18** 2945
[40] Li Y L, Fan W L, Sun H G, Cheng X F, Li P, Zhao X, Hao J C and Jiang M H 2010 *J. Phys. Chem. A* **114** 1052
[41] Babu K R, Lingam C B, Auluck S, Tewari S P and Vaitheeswaran G 2011 *J. Solid State Chem.* **184** 343
[42] Furno M, Meerheim R, Hofmann S, Lüssem B and Leo K 2012 *Phys. Rev. B* **85** 115205